Linked Modeling of Phase Evolution and Transformation during Solidification and Homogenization of Ternary Al-Alloys

Th. Hofmeister, K Greven, A. Ludwig, P.R. Sahm
Foundry Institute, RWTH-Aachen
Intzestr. 5, D-52056 Aachen, Germany

Abstract

The microstructure determines for the most part mechanical properties of castings. This is the case especially with age-hardening aluminum alloys. To predict the phase transformation in cast parts during and after solidification a sophisticated approach to a coupled modeling of various simulation phenomena is presented. This approach couples a diffusion equation solver which considers the online estimation of thermodynamic equilibria with a macroscopic model for temperature and stress calculation. The macroscopic calculations were performed by means of the in-house 3D-FEM program CASTS. It enables the simulation of the temperature distribution in castings taking into account various initial and boundary conditions. The coupled micro-model predicts the dendrite solidification of ternary alloys. It characterizes important microstructural features like dendrite arm spacing and the amount of fraction eutectic. Effects like solid state back diffusion, dendrite arm coarsening and tip undercooling are considered. The homogenization of this microstructure is simulated in a following step by using a further subroutine. Phase diagram information for a multicomponent system is provided on-line by ChemApp™. Permanent mould casting experiments with ternary aluminum alloys are used to validate this new approach.

Modeling of Casting, Welding and Advanced Solidification Processes IX
Edited by Peter R. Sahm, Preben N. Hansen and James G. Conley

1. Introduction

Age-hardening aluminum alloys are a common material both in the automobile and the aerospace industry. The main feature of this material is the extreme hardness in relation to the density. Discovered in 1938 the crystallographic basis for age-hardening is the creation of a precipitation structure that severely strains the solvent matrix and thereby causes hardening. These days numerical investigations of casting processes are quite usual. On the macroscopic level they allow the global prediction of mold filling, solidification and stress formation. Some numerical techniques on the micro level have been developed to predict the local evolution of microstructure and the formation of microsegregation as a function of the global cooling conditions. Reviews of analytical, semi-empirical and numerical methods can be found in [1,2]. As demonstrated by Boettinger et al. [3,4], the on-line use of thermodynamic programs is advisable to enhance the accuracy of thermodynamic data for multi-component alloys. Micro and macro models should ideally be closely coupled to take into account mutual influences between microstructural evolution, temperature changes and the stress formation during solidification and subsequent cooling. This work presents a coupled modeling of the solidification, the microstructure and residual stresses, an approach to simulate the homogenization, as the first step in the age-hardening process, and nevertheless some experimental work.

2. Numerical Procedure

The described simulations on the macro level are performed by means of the in-house package CASTS, a 3D finite element code. Detailed descriptions and application examples can be found in [5,6,7]. The mesh can be generated with either a commercial software or with an in-house net generator. To realize the interfacial heat flow, additional elements are enmeshed between different materials. After defining temperature-dependent thermophysical properties and setting appropriate initial (e.g. pouring temperature) and boundary conditions (convection, insulation and radiation including view factors) all information is stored in a command file. During the mainprocessing the program calculates the temperature evolution using iterations. According to the combined heat, stress and microstructure simulation the release of latent heat, which is evaluated by the micromodel, and the heat transfer between mold and casting, calculated in the stress module, is taken into account.

2.1 Constitution of the Al-Cu-Mg-System

Al-Cu-Mg is a typical age-hardening alloy. Due to the low density and the relative hardness and strength it is often used in the automobile- and aerospace-industry. The solidification of a AlCu4Mg-alloy starts in the Al-rich corner with the solidification of α–dendrites, **Figure 1**. The eutectic groove is reached at an amount of 34wt%Cu in the liquid. At this point α– and θ-phase (Al_2Cu) solidify. Finally at 502°C the ternary point is reached. The remaining liquid changes into α-, θ- and S-phase (Al_2CuMg), **Figure 2**. In the liquid the diffusion of magnesium may be slightly increased by copper additions. In the solid state neither copper nor magnesium affects appreciably the other element diffusion.
Hardness, ultimate tensile strength, yield strength and percentage elongation are strongly dependent on heat treatment. Fatigue strength is very sensitive to age hardening: it is maximum before the intermediate phase forms and minimum at the end of precipitation, when the Al_2CuMg-phase is present as sharp-cornered platelets. In alloys in which the copper/magnesium ratio is more than 8:1 the main hardening agent is Al_2Cu, in alloys in the range 8:1 to 4:1 both Al_2Cu and Al_2CuMg are active. Between 4:1 and 1.5:1 Al_2CuMg controls the properties. Precipitation in aluminum-copper-magnesium-alloys with $C_{Cu}/C_{Mg}>2$ starts with the formation of GP zones, consisting of a segregation of copper and magnesium atoms. The increase in volume at the beginning of aging, which is then followed by a decrease, has been interpreted to indicate, respectively, the formation

of disordered zones and their ordering. The ordered zones, also designated S", are still coherent with the matrix as they grow in the matrix direction. Eventually there is a rearrangement within the S" zones, to form the transition phase S'. It is still coherent with the matrix and can grow to more than 10 nm thickness. Eventually the S' phase grows to a point that loses coherency with the matrix and the S (Al_2CuMg) precipitate replaces it.
The effect of solution treatment temperature is normal: too low a temperature leads to incomplete solution and reduced aging. Most commercial alloys are at the saturation limit and require maximum solution temperatures, but the Al-Al_2Cu-Al_2CuMg eutectic limits the temperature to 775 K. [8]

2.2 Simulation of Solidification Microstructure

The microsegregation model predicts primary dendrite trunk spacing, λ_1, secondary dendrite arm spacing, λ_2, and phase amounts. Complete mixing is assumed in the liquid and the volume element is thought to be at a uniform temperature T. In the solid the concentration profiles of both alloying elements are calculated by solving Fick's second law. All information concerning the phase diagram was calculated with the aid of the programmable thermodynamic calculation interface ChemApp™ [9]. It consists of FORTRAN subroutines that allow the calculation of thermodynamic equilibria by minimizing the Gibbs free energy. These subroutines are directly coupled with the simulation program.
Two models taking into account solid-state diffusion have been integrated in addition to the lever rule and the Gulliver-Scheil model to calculate the microsegregation. One phase solidification uses the approach of Roósz and Exner [10] where the complex dendrite structure is approximated by a plate morphology. Dendrite arm coarsening and dendrite tip undercooling is considered. Eutectic solidification is calculated with a modified model of Chen and Chang. The complete microstructure model is shown in, **Figure 6**. At each time step and each nodal point the microstructure calculation is called up. After the calculation of the thermal gradient, at all nodes within the solidification range, the undercooling of the dendrite tip ΔT^*, consisting of curvature, solutal and gradient undercoolings, is calculated on the basis of the KGT-model. It is considered in the micro model by using the method of Voller and Sundarraj [11]. If the solidification starts at one point the latent heat is calculated corresponding to the models for one-phase and eutectic solidification.
Figure 7 shows the one-phase simulation. In this case the temperature alone is not sufficient to fix the definite state in the phase diagram. Thus the mass balance of both alloying elements is used. Two independent iteration loops guaranty the keeping of this balance.
Figure 8 shows the course in the case of eutectic solidification. In the eutectic groove, the growth of primary α-dendrites is assumed to be completed while the secondary α- and β-phases solidify. The main point of this subroutine is the iterative solving of the equation matrix consisting of mass balances and continuum equations. The initial value of the iteration is determined using the Gulliver-Scheil model. Different time steps $\Delta t_{micro} = \Delta t_{macro}/N$ and different sub-relaxation factors ϕ are used depending on the different cooling conditions at the different nodes to secure the convergence of the iteration. Therefore the developed solution algorithm starts at each nodal point of the geometry with the numerical values N=1 and ϕ=1. In the case of divergence both N and ϕ will be varied until convergence is reached. Within the microstructure calculation interpolated temperature values of the macro program are used.
Micro and macro programs are linked via the local release of latent heat at each node of the mesh, similar to the method of Sasikumar et al. [12]. At the beginning of each time step t the iteration loop starts with an estimated fraction solid, f_s, for all nodes i. It determines the release of latent heat from the macro calculation. With this evaluated temperature distribution $T^0_{n,i}(t)$ the micro model simulates the microstructural evolution, leading to a better approximation of f_s which is again input for a repeated macro calculation. This procedure is repeated until sufficient agreement between the temperature distribution of the actual and previous iteration is obtained.

2.3 Simulation of Stress and Distortions

Thermal stresses are due to a hindered shrinkage of the casting and inhomogeneous cooling conditions. Based on the calculated time dependent temperature field total strains and stresses are calculated incrementally. The stress simulation switches between a global and a local level. The displacements at a time step *t* are calculated at the global level. A unified constitutive law predicts the strain rate depending on the actual temperature *T* and microstructure as well as the current build up creep and plasticity state of the cast material. In order to take the mechanical interactions between mold and casting into consideration a gap/contact approach was integrated which applies the same interface elements that are used within the temperature calculation. A detailed description can be found in [7]. Unlike others methods the mold is not assumed to be rigid.
This approach simplifies the appropriate setting of mechanical boundary conditions since it checks at each time step for each interface node whether a gap between mold and cast part exists or local contact forces have to be accounted. Depending on the stage of shrinkage an algorithm controls closing and opening of adjacent interface nodes by manipulating the global stiffness matrix. In cases when classical procedures like the penalty-method or the use of LaGrange multipliers may lead to numerical problems this approach is numerically stable and accurate but increases the necessary computation time up to 30 %.

2.4 Simulation of Homogenization

The first step in age-hardening is the homogenization of the casting texture. It is the basis for the following precipitation and heat treatment. With the described simulation step only the homogenization is simulated. It predicts the remaining phase amounts. After the solidification simulation is completed, the dendrite arm coarsening and the interchange of latent heat with the macro program are not taken into consideration. Two coupled calculations are implemented. The first treats the dissolution of θ–phase into the α–phase. The half eutectic lamellar spacing is taken as basis for the maximum diffusion range. So the cell size for considering the θ–phase dissolution is around 1 µm. Thus the lever-rule is used to calculate the average alloy-element-concentration in the α–phase. These results are integrated into a calculation treating the liquidation of the S-phase and the diffusion of Cu and Mg into the α–phase. According to the dendrite arm spacing in this model, the cell size for considering the liquidation of the S-phase is about 20µm. The concentration trend is calculated with a diffusion model respecting the current diffusion coefficients.

3. Results and Discussion

The results of two different castings will be discussed. To validate the described numerical procedure and as there still has not been experimental work with the actual casting, an U-bar, **Figure 4 and 5** show the results of experimental and simulation work with the former casting, a step wedge, **Figure 3**. It is obvious that there is a good agreement between calculation and measurement for λ_a especially at positions where a fine microstructure occurs. The deviation between the simulation and experiment for the large values of λ_a may be explained by two different reasons. First, measurements especially on coarse microstructures reveal an unavoidable scatter. Second the material properties especially the diffusion coefficient in the considered ternary alloy are not known precisely. The α–phase distribution shows a good correspondence between experiment and simulation. All four samples measured by using a X-ray-analysis are very close to the simulated values. A former optical analysis also showed that the tendency of a decreasing α–phase volume fraction, beginning from the outside of the casting to the inside, is represented in the simulation.
Figure 10 to 16 show the results of the U-bar microstructure simulation. The FEM-net contains 1144 nodes including the mold. 242 nodes are needed for the U-bar, **Figure 9**. One fully coupled simulation took about 24 hours on an SGI™ workstation with R12000 processor. Displayed results are the microstructure parameters λ_d ,**Fig. 15**, and λ_a ,**Fig. 16**, and the distribution of the amounts of the Al-rich α-phase ,**Fig. 12**, the θ-phase (Al_2Cu) ,**Fig. 13**, and the S-phase (Al_2CuMg) ,**Fig. 14**,

for an AlCu4Mg-alloy. As expected, in those parts of the casting where high solidification velocities occur (primarily in the thinner side panel) a fine microstructure develops. On the other hand in the bulk material a coarse microstructure occurs. The phase distribution is very homogenous. Generally the amount only varies in a very small range. In the whole casting there is not less than 97% α-phase and not more than 1.3% S-phase.
Stress and distortion in the casting after solidification show their maximum in the ground panel where the solidification ends and in the transition to the side panels, **Fig. 11**.

4. Conclusions

Numerical results of the simulation of a casting process with a coupled treatment of stresses, temperatures and microstructure formations are presented. The simulation provides precise information about the temperatures, residual stresses, dendrite trunk and arm spacing and the distribution of the occurring phases after solidification. By comparing the simulation with experimental data the applicability of the used models is proved. To validate the homogenization simulation experimental investigations are in progress.

Acknowledgement

This research was sponsored by the German Science Foundation (DFG) within the framework of the collaborative research center SFB 370 for which the authors wish to express their gratitude.

References

[1] M. Rappaz, Int. Mater. Rev. 34 (1989), 93-123
[2] T. Kraft, H.E. Exner, Z. Metallkd. 87 No. 8 (1996), 598-611 and 652-660
[3] W.J. Boettinger et al., in *Proc. of Int. Conf. Modeling of Casting, Welding and Advanced Solidification Processes VII*, ed. M. Cross, J. Campbell (1995), 649-656
[4] H.E. Exner, M. Rettenmayr, A. Roosz, Mat. Sci. Forum 77 (1991), 205-210
[5] P.N. Hansen, P.R. Sahm, in *Proc. of. Int. Conf. Modeling of Casting and Welding Processes IV*, ed. A.F. Giamei , G.J. Abbaschian (1988), 529-542
[6] M. Fackeldey et al., in *Proc. of 4th Decennial Int. Conf. On Solidification Processing*, Sheffield (1997), 41-44
[7] M. Fackeldey, A. Ludwig, P.R. Sahm, Comp. Mater. Sci. 7 (1/2) (1996), 194-199
[8] L.F. Mondolfo, Aluminum alloys, structures and properties, Butherworths (1976), 497-504
[9] Eriksson G., Spencer P.J., Sippola H, in *Proceedings 2nd Colloquium on Process Simulation*, Helsinki University of Technology, Report TKK-V-B104 (1995) 113
[10] A. Roósz, E. Halder, H.E. Exner, Mater. Sci. Tech. 2 (1986), 1149-1155
[11] V.R. Voller, S. Sundarraj in *Proc. of Int. Conf. Modeling of Casting, Welding and Advanced Solidification Processes VI*, ed. T.S. Piwonka, V. Voller, L. Katgerman (1993), 251-258
[12] R. Sasikumar, H.E Exner, Modeling Simul. Mater. Sci. Eng 1 (1992), 19-27

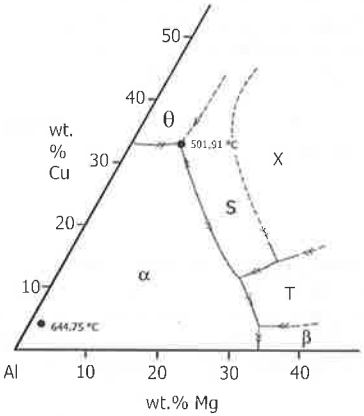

Figure 1: Al-rich corner in the Al-Cu-Mg-system

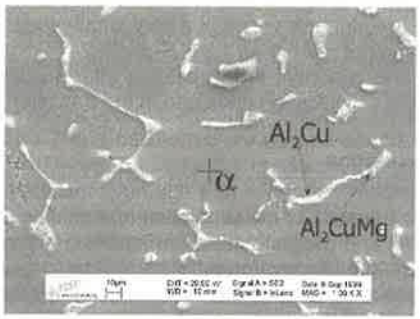

Figure 2: Phase distribution in a AlCu4Mg sample

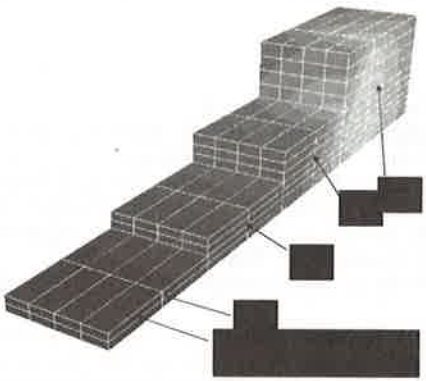

Figure 3: Simulated half step wedge with sample locations

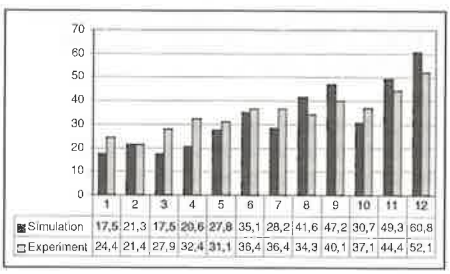

Figure 4: Comparison of measured and simulated values of the dendrite arm spacing λ_a. All quantities in µm.

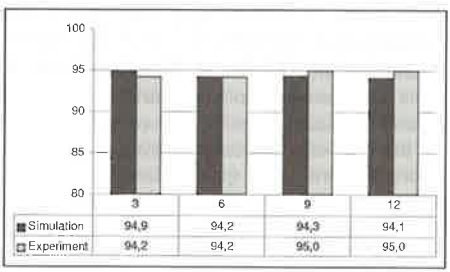

Figure 5: Comparison of measured and simulated values of the α-phase. Quantities given in vol. %.

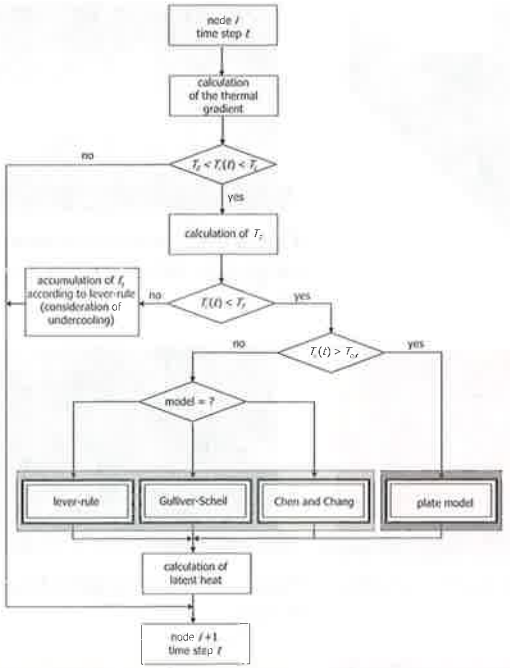

Figure 6: Scheme of the microstructure model

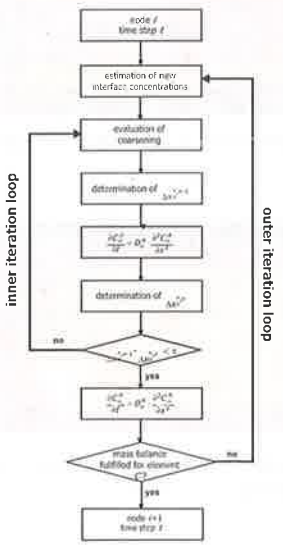

Figure 7: Subroutine for the microstructure calculation during one-phase solidification.

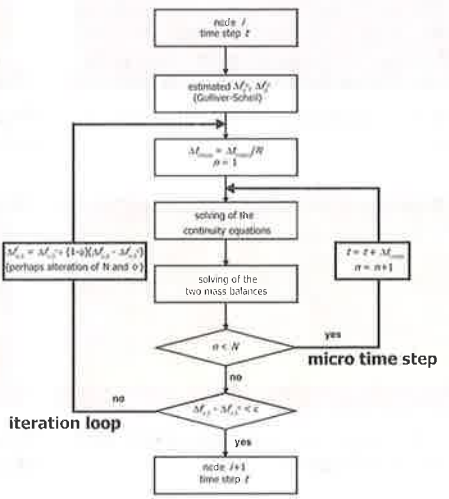

Figure 8: Subroutine for the microstructure calculation during eutectic solidification.

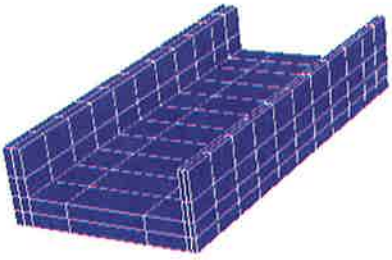

Figure 9: Casting "U-bar"

Figure 10: Temperature distribution [scale range from 380-510°C] Isothermal line at 507°C

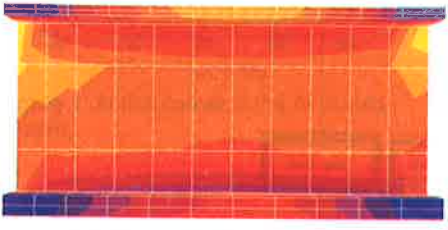

Figure 11: Stress distribution after solidification [0-250 MPa]

Figure 12: α-phase [97,0-97,4%] after solidification

Figure 13: θ-phase [1,4-1,6%] after solidification

Figure 14: S-phase [1,1-1,3%] after solidification

Figure 15: Dendrite trunk spacing [100-230 µm] after solidification

Figure 16: Dendrite arm spacing [10-35 µm] after solidification